**Natural Hazards manuscript No.**
(will be inserted by the editor)

# Visualizing Uncertainties in a Storm Surge Ensemble Data Assimilation and Forecasting System

**Thomas Höllt · M. Umer Altaf · Kyle T. Mandli · Markus Hadwiger · Clint N. Dawson · Ibrahim Hoteit**

Received: date / Accepted: date

**Abstract** We present a novel integrated visualization system that enables the interactive visual analysis of ensemble simulations and estimates of the sea surface height and other model variables that are used for storm surge prediction. Coastal inundation, caused by hurricanes and tropical storms, pose large risks for todays societies. High-fidelity numerical models of water levels driven by hurricane-force winds are required to predict these events, posing a challenging computational problem and even though computational models continue to improve, uncertainties in storm surge forecasts are inevitable. Today this uncertainty is often exposed to the user by running the simulation many times with different parameters or inputs following a Monte-Carlo framework in which uncertainties are represented as stochastic quantities. This results in multidimensional, multivariate and multivalued data, so-called ensemble data. While the resulting datasets are very comprehensive, they are also huge in size and thus hard to visualize and interpret.

In this paper we tackle this problem by means of an interactive and integrated visual analysis system. By harnessing the power of modern graphics processing units (GPUs) for visualization as well as computation, our system

T. Höllt, M.U. Altaf, M. Hadwiger, I. Hoteit
King Abdullah University of Science and Technology, Thuwal, Saudia Arabia
4700 KAUST
Al-Khwarizmi Building (1), Room No. 4415
Thuwal 23955-6900
Kingdom of Saudi Arabia
Office: +966 28080344
E-mail: thomas.hollt@gmail.com,
{umer.altaf|markus.hadwiger|ibrahim.hoteit}@kaust.edu.sa

K.T. Mandli*, C.N. Dawson
Institute for Computational Engineering and Sciences, University of Texas at Austin, Austin, Texas
E-mail: {kyle|clint}@ices.utexas.edu
*Presently at Columbia University in the City of New York, New York, NY.
*E-mail: kyle.mandli@columbia.edu*

allows the user to browse through the simulation ensembles in real-time, view specific parameter settings or simulation models and move between different spatial or temporal regions without delay. In addition our system provides advanced visualizations to highlight the uncertainty, or show the complete distribution of the simulations at user-defined positions over the complete time series of the prediction. We highlight the benefits of our system by presenting its application in a real world scenario using a simulation of Hurricane Ike.

## 1 Introduction

Coastal inundation due to hurricanes and typhoons pose large risks for todays societies, causing a large number of deaths all over the world. The death toll caused by the Bhola cyclone surge, which made landfall in Bangladesh in November of 1970, is estimated between 300,000 and 500,000 people (Murty et al, 1986). Hurricane Katrina killed at least 1,200 people when it made landfall in Louisiana and Mississippi in 2005 (Blake et al, 2011). Just recently, in 2013, the Haiyan Typhoon in the Philippines caused over 6,000 deaths. Authorities can benefit greatly from accurate numerical forecasts of coastal flooding providing important information for evacuation planning and deployment of emergency personnel.

The study of storm surge is not new and dates back several decades (Heap, 1983). Dietrich et al (2010, 2011a) as well as Kennedy et al (2011) and Hope et al (2013) recently investigated the most severe U.S. hurricanes, including Hurricane Katrina, Rita, Gustav, and Ike using hindcasting studies. These hindcast studies are based on the coupled SWAN+ADCIRC hydrodynamics model, described by Dietrich et al (2011b). This modeling framework is also now routinely used in prediction as hurricanes approach land; see Dietrich et al (2013) and the references therein for a description of the ADCIRC Surge Guidance System.

Uncertainties in numerical predictions of storm surge are inevitable (Brown et al, 2007; Butler et al, 2012). These may be due to the poor knowledge of the hurricane characteristics (track, wind speed, forward speed, etc.) and physical parameters and inputs such as bottom friction and bathymetry. Measurements of storm surge such as satellite and in-situ measurements of water levels and currents are now more readily available in real-time. This data can be assimilated into the model to improve its behavior and to reduce the uncertainties in the model outputs (Ghil, 1989; Malanotte-Rizzoli et al, 1989). This process is called data assimilation.

Data assimilation uses incoming data sequentially as they become available to update the model predictions and associated uncertainties. Here we propose an advanced visualization system that summarizes the most important information about the distribution of the simulation output. The system provides an interactive framework to interpret the uncertainties in space and time and would allow for efficient and timely analysis of the system outputs for risk management and decision making.

The literature divides data assimilation methods in two classes: variational methods and sequential methods. Variational methods are least-squares fitting methods, which use optimization algorithms to improve the model fit with data. Sequential methods are based on the Bayesian filter which computes the distribution of the system state given the observations in two steps: a prediction step to propagate the distribution forward in time and an update step of the distribution with incoming data (Lermusiaux et al, 2006; Hoteit et al, 2008). One can then compute any statistical quantities of the system state, including different estimate and associated uncertainties.

The need for uncertainty quantification and ensemble simulation and computation is now recognized in many areas such as, but not limited to, ocean and weather forecasting as described above, climate prediction (Cubasch et al, 1994) and engineering (Helton, 2008). Ensemble simulations provide much more information to domain scientists than traditional single run simulations. To efficiently analyze these ensemble simulations, which typically result in huge amounts of data, scientists rely on computational support. This can be completely automatic, such as that provided by data mining techniques or statistical analysis, or by means of interactive visual tools.

Some of the earlier work by the visualization community was presented by Pang et al (1997) which provides a good introduction to visualization of data and their corresponding uncertainties. They categorize uncertainty based on its origin, such as acquisition or transformation, and provide a mapping of existing visualization techniques to uncertainty visualization based on the application. Johnson and Sanderson (2003) as well as Griethe and Schumann (2006) provide overviews of different uncertainty visualization techniques for spatial 2D and 3D scientific data, such as surface data, as well as more abstract data. Griethe and Schumann (2006) define a set of basic concepts of uncertainty in visualization. Riveiro (2007) evaluates different uncertainty visualization techniques in the context of information fusion. Uncertainty information in spatial data can be visualized with a multitude of techniques. Color and texture are especially suited for surface data, such as iso-surfaces (Rhodes et al, 2003). Texture also works well to highlight uncertainty in volume renderings of 3D data. Another common approach to show uncertainty in 3D data is by introducing noise. Djurcilov et al (2001, 2002) show the effectiveness of both approaches in the context of ocean simulations. Pöthkow and Hege (2011); Pöthkow et al (2011) as well as Pfaffelmoser et al (2011) extend surfaces to cloud like structures to visualize the spatial variation, corresponding to the uncertainty in probabilistic iso-surfaces. Brown (2004) shows the utility of animation in the context of uncertainty visualization, arguing that animating through possible results will show a steady behavior in certain areas, while uncertain regions will show large variation.

Uncertainty visualization constitutes the basis of ensemble visualization. Here the uncertainty is derived based on statistics computed on the multivalued part of the ensemble data. Early work on ensemble visualization, though not under this term, was conducted by Pang, Kao and colleagues (Kao et al, 2001, 2005; Luo et al, 2003; Love et al, 2005). Standard visualization techniques

were adapted to so called spatial distribution data gathered from various sensors, e.g. satellite imaging or multi-return LIDAR. The authors define spatial distribution data as collections of multiple values for a single variable in multiple dimensions, which is essentially the definition of ensemble data. These kind of data is gathered today for vastly different applications in various forms such as measurements from sensors as described above. Höllt et al (2013a) describe a system that uses optimization techniques for subsurface analysis producing ensemble data which is distinctively non-Gaussian, and as such can not be represented easily in a parameterized form. Nowadays weather forecasts essentially are all based on ensemble simulations, hence it is not surprising that some of the early integrated systems for ensemble visualization target this specific application. *Ensemble-Vis* by Potter et al (2009) as well as *Noodles* by Sanyal et al (2010) are just two examples that were designed specifically to allow efficient analysis of ensemble weather prediction simulations. Besides specialized visualization techniques focusing on the most important features of the data for domain scientists they share the use of multiple linked views to allow interactive exploration of multidimensional, multivariate and multivalued ensembles. In recent work Höllt et al (2013b, 2014) presented one of the first integrated systems for the visual exploration and analysis of ensemble data specifically targeting ocean forecasts. The presented system can handle time-series of multivalued ensembles of sea surface height data, represented by regularly sampled 2D height fields. A set of statistical properties is derived from the ensemble and can be explored in multiple linked views, while the complete ensemble remains directly accessible for detailed inspection on demand. The system enables domain experts to efficiently analyze ocean predictions, including their corresponding uncertainties. The goal is to provide aid in planning the placement and operation of off-shore structures such as oil platforms and underwater vehicles such as gliders.

In this work we generalize the framework to the specific needs of storm surge analysis such as handling unstructured grids. By using the GPU for computation as well as visualization we allow real-time exploration of this data.

The remainder of this paper is structured as follows. Section 2 gives a brief introduction of the storm surge assimilation and prediction system. Section 3 presents the visualization system and it's capabilities (Sections 3.1 and 3.2) as well as an overview of the implementation and data handling (Section 3.3). In Section 4 we present a case study, based on a forecast of Hurricane Ike, demonstrating the application of our system in a real world scenario. Section 5 concludes with the key findings and an outlook on future work.

## 2 Storm Surge Assimilation and Prediction System

### 2.1 The storm surge model

The Advanced Circulation (ADCIRC) model (Luettich and Westerink, 2005) solves the two-dimensional shallow water equations on an unstructured grid using a finite element approach. The unstructured grid allows the model to resolve coastal features while not overly resolving the deeper ocean. One common area of application of the ADCIRC model has been the Gulf of Mexico where it has been used in a hindcast context to validate the model, *e.g.* see Westerink et al (2008); Bunya et al (2010); Dietrich et al (2010); Kennedy et al (2011); Hope et al (2013). ADCIRC is also run in a forecast configuration where best-track data from the National Hurricane Center (NHC), which includes location and intensity parameters for a particular storm forecast, is used to construct a parameterized storm field. For the theoretical, numerical, algorithmic, and high performance computing developments of the ADCIRC model, we direct the interested readers to Luettich and Westerink (2005).

### 2.2 The assimilation and uncertainty quantification approach

Numerical implementations of the Bayesian filter are based on ensemble methods, mainly the Ensemble Kalman filtering (EnKF) method, which propagates the state distribution forward in time using an ensemble-based Monte-Carlo approach, and applies Gaussian-based Kalman update step to the ensemble with incoming observations (Evensen, 1994; Hoteit et al, 2005). Recently EnKF methods have become very popular in many geophysical applications, thanks to their robustness, efficiency, reasonable computational cost, and their ease of implementation. Different EnKF methods are proposed in the literature. Tippett et al (2003) divide these methods into two groups; the stochastic EnKF (SEnKF) and the deterministic EnKFs (DEnKFs). In the SEnKF, described by Burgers et al (1998) and Houtekamer and Mitchell (1998), the observations are perturbed before the Kalman update step is applied to each predicted ensemble member. DEnKF techniques do not perturb the observations but rather use a specific square-root form of the ensemble sample error covariance matrix in combination with the ensemble mean for each update step. Different variants of DEnKFs were introduced by for example Anderson (2001), Bishop et al (2001), Whitaker and Hamill (2002), and Hoteit et al (2002). The public availability of the DEnKF codes helped increasing the popularity of these filters. One of them is the singular evolutive interpolated Kalman (SEIK) filter (Pham, 2001; Hoteit et al, 2002), which as shown by Nerger et al (2012), follows a similar formulation to the ensemble transform Kalman filter (ETKF) presented by Bishop et al (2001).

Heemink (1986) introduced a steady-state Kalman filter which was specifically developed to enhance storm surge prediction and was later used in multiple applications as presented for example by Heemink and Kloosterhuis (1990),

Sørensen and Madsen (2006) and El Serafy and Mynett (2008). This approach, however, is limited by two constraints; it requires an invariant observation network and does not address system nonlinearity. The SEIK filter was incorporated into the short range ADCIRC prediction system (Butler et al, 2012; Altaf et al, 2013) to overcome these problems. It was concluded that the filter worked effectively and considerably improved the short range forecasts, which is subject to a unique fast-evolving dynamics typical of an extreme event. Recently Altaf et al (2014) investigated the performances of the most common EnKFs for data assimilation into an ADCIRC storm surge model using data from Hurricane Ike and concluded that these filters would eventually lead to comparable performances when properly tuned.

## 3 Visual Analysis System

The goal of our visualization system is to enable interactive exploration and visual analysis of multi-valued sea surface height (SSH) data using a combination of automated statistical analysis and interactive visualization of the results of this analysis. Section 3.1 describes the statistical analysis as implemented in our system, while Section 3.2 gives an idea on how the combination of multiple linked views, as shown in Figure 1 enables the interactive visual analysis of the ensemble data.

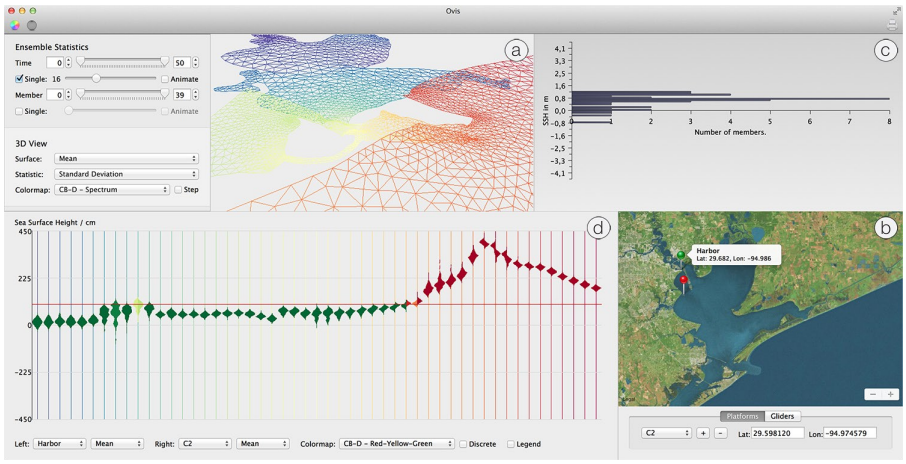


**Fig. 1 System Overview.** Our system for exploration of ocean prediction ensembles consists of four main views. The simulated ocean surface, or a derived version like the mean surface for a single point in time, can be shown in 3D or 2D (a) and (b). The histogram view (c) shows the complete distribution of the ensemble at a selected position, while the time-series view (d) shows the distribution and the resulting operational risk at a selected position for multiple samples along time.

### 3.1 Statistical Analysis

The foundation for the visual analysis builds on an extensive statistical analysis of the members of the ensemble data. We compute the statistics for each point of the grid separately. At each point of the grid, every member of the ensemble provides a value for the sea surface height. While the probability for every member is set uniformly, some members have the same or similar values resulting in higher probabilities for these values. The first step in our statistical analysis is the creation of histograms of the SSH for each position in the grid. Based on these histograms, a probability density function (pdf) is approximated using a kernel density estimate. We assemble these 1D histograms and pdfs in an indexed array, corresponding to their position, so that the user can look up each pdf directly when needed.

In addition to the histogram and pdf, which provide detailed information on the distribution at any given grid point, we compute scalar properties for each position, such as range, mean, median, maximum mode, standard deviation, variance, skewness, and kurtosis. Assembled at their corresponding positions of the grid, these values can semantically be divided into two different categories; mean, median and maximum mode describe the sea surface height and can thus be used as possible results or representatives for the SSH, the other scalars provide meta information on the distribution of the ensemble and can be used to augment the former. A combination of these two categories is typically used to provide a basic overview of the ensemble. For example a common approach would be to show the mean SSH as a probable prediction and augment it with the standard deviation of the spread of the ensemble to indicate the uncertainty. In our system this might be done for example by showing the mean SSH as an actual surface in 3D and use color-mapping to augment it with the meta information, such as the standard deviation. More details are given in Section 3.2 below.

To allow an efficient exploration of the complete ensemble we made the statistical analysis completely visualization-driven. The consequences of this are twofold: First, on the implementation side, statistics are only computed on-the-fly when needed for visualization. More importantly, the on-the-fly computation enables interactive visual exploration of the ensemble and the corresponding parameter space. As described above the statistical analysis is carried out on the complete ensemble. However, since the computation happens on-the-fly the user can define any desired part of the ensemble to analyze. Members can be removed on-the-fly, subranges can be selected, etc. This allows an interactive exploration of the parameter space that was used for simulating the ensemble.

To enable this continuous real time re-computation of the statistics we implemented a completely GPU-based pipeline not only for visualization but also for computation (see Section 3.3 for the implementation details).

### 3.2 Visual Prediction Exploration

The goal of this work is to provide an integrated system for the analysis and interpretation of storm surge predictions gained from ensemble simulations and data assimilation. We provide a set of different views for the different tasks of the analysis. Figure 1 shows our application with the four main views plus a unified settings panel. Two of the views are spatial, showing the surface data themselves, one in 3D (Figure 1(a)), the other one in 2D (Figure 1(b)). A linked histogram view (Figure 1(c)) shows the histogram as described above for selected grid points. The time-series view (Figure 1(d)) provides detailed information for a user-defined set of positions in time and space.

***2D View.*** Most domain scientists working with spatial 2D data are comfortable with 2D views as shown in Figure 1(b). In our system it is used to obtain an overview of the data, either directly by showing the complete scalar field using pseudo coloring, or indirectly by plotting iso-contours extracted for user defined values from the selected scalar field. While our system allows free configuration to directly or indirectly visualize any desired statistic, the most common setting is using iso-contours to show important values for the mean SSH for a selected assimilation cycle and augment it with the standard deviation mapped to pseudo coloring to indicate uncertainty.

The 2D and 3D views are also used for user interaction, allowing direct manipulation of selected positions of special interest, e.g. to select a position that shall be investigated in the histogram or time-series view.

***3D View.*** 3D visualizations are used less frequently mainly because they need to be projected back to 2D for common display devices. However since 3D visualization provides one more degree of freedom, compared to 2D, it can provide additional information. In the 3D view (Figure 1(a)) in our system, the sea surface height naturally maps to the height- or z-dimension of the view, meaning pseudo-coloring and iso-contouring can be used to augment the SSH with two additional statistical properties. To overcome the downsides of projecting back into 2D we start with a top down view, resembling the 2D view, but the user can freely navigate in the 3D view in real-time, allowing inspection of the data as needed.

***Histogram View.*** Figure 1(c) shows the histogram view that is used to provide insight on the complete distribution of the simulated SSH values at a selected position in space and time. Unlike a conventional histogram that usually maps the bins to the $x$-axis and the corresponding values to the $y$-axis we use a layout rotated by 90 degrees. Since we are using the histogram to show the distribution of height values it is natural to use the $y$-axis to indicate the height. This also provides a spatial context since we can position the histogram bins according to the actual height. This concept makes even more sense in the time-series view described below, where multiple glyphs can easily

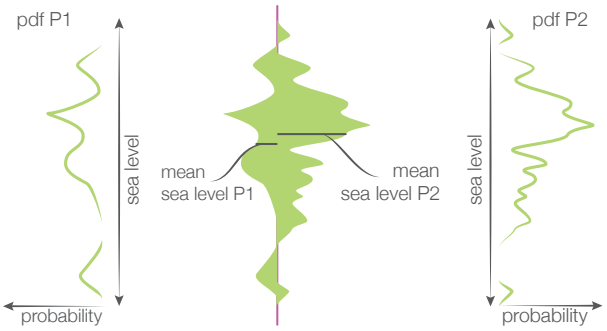


**Fig. 2** The **Time-Series View Glyph** in detail. The sides of the glyph show the pdf of the distribution for selected positions in time and space. The user can configure the glyph to show the distributions of two different positions on the two sides of the glyph. For the time-series view the glyphs for all positions in time are assembled next to each other, allowing the user to inspect the complete time-series for one or two positions in space at once. When defined properly the glyph can also show other distribution data, like the distance to the surge for each ensemble member.

be compared when they are displayed next to each other using the same height axis.

The spatiotemporal position is selected by setting the desired assimilation cycle via the general GUI. The $(x, y)$-coordinate can then be selected by directly picking the position in one of the spatial views.

***Time-Series View.*** Going a step further from showing the histogram for a single position in space and time, the time-series view (Figure 1(d)) enables the user to inspect the complete temporal evolution of the distribution at a single position in space over time. Therefore we use a glyph (Figure 2), described below in detail, that conveys the most important features of the distribution, including the complete histogram, at a selected position. Using such a compact representation allows us to assemble the glyphs for multiple assimilation cycles in a single view to show the complete evolution over time.

Figure 2 shows a detailed description of the glyph, which is inspired by the violin plots, introduced by Hintze and Nelson (1998). While the shape of the violin plot is symmetric, the left and the right side of the glyph can be defined via two different properties. This setup enables two configurations; either the two sides of the glyphs can be used to show two different properties of the same spatial position or to compare the same property, such as the SSH at two different points of the grid. In the example in Figure 2, we show the sea surface height for two different positions. We map the pdf of the sea surface height as described in Section 3.1 for each position on one side of the glyph. The glyph could also be used to show other properties, like the distance to the storm surge front for every ensemble member. However, since the most important application is displaying sea surface height distributions, we decided to use the same vertical layout as described above for the histogram view. The glyph

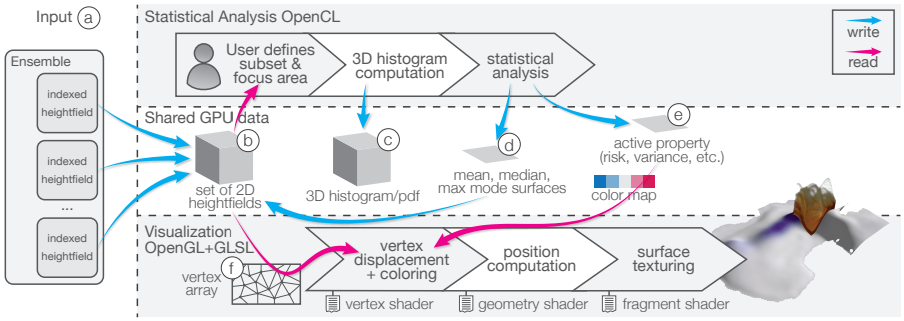


**Fig. 3 Pipeline Overview.** The pipeline is divided into two major blocks: The statistical analysis part at the top, and the rendering part shown at the bottom. Both parts are entirely GPU-based, and all data (middle row) are shared by both parts in GPU memory. Keeping the complete dataset on the GPU and sharing the data between the processing and visualization pipelines allows to utilize the full performance of the GPU.

is positioned on the y-axis according to the actual height values, making the position not only comparable to other glyphs at different positions in the view, but also to a user-defined threshold, which could for example indicate a sea level were a certain area might be flooded. The mean values of both properties are indicated by a black bar on their respective sides of the glyph. Additionally, the glyphs are pseudo-colored according to a user selected statistical property, derived from the data. A very useful property in this view is the probability that the sea level at the position reaches, or surpasses, the critical sea level discussed above. Information on the uncertainty of the data can immediately be retrieved from the shape of the glyph: A large spread or variation in the surface positions over the ensemble, indicating larger uncertainty, results in a large glyph, while little uncertainty results in less variation and more compact glyphs.

### 3.3 Implementation

To enable interactive updates the statistics computation as well as the visualization are executed in an integrated GPU-pipeline. The analysis and visualization pipeline is illustrated in Figure 3. The pipeline is divided into two main parts: The statistical analysis (upper third of the illustration) is implemented using the general purpose GPU programming API OpenCL (Munshi et al, 2011), while the visualization is based on OpenGL (Shreiner et al, 2013) in combination with custom shaders written in the OpenGL Shading Language (Rost et al, 2009). Recent versions of these APIs allow sharing the data on the GPU between both parts of the pipeline, avoiding costly data transfers. The readers are referred to Höllt et al (2014) for more details. In the following we give a brief overview of the implementation and highlight the changes made to support the storm surge data.

***Input.*** The input to our system (Figure 3(a)) is an ensemble of sea surface height simulations. Where the original work by Höllt et al (2014) assumed the data to be on a regularly sampled grid, the storm surge simulations require unstructured grids to implement a much higher precision in the coastal regions. Therefore we index the input data and use the index and not the $(x, y)$-coordinate for accessing the data. The index is also used as the correspondence between ensemble members.

***Data Representation.*** To enable the irregular grids used for storm surge predictions we represent the data by means of two data structures with the same indexing. First, the positional information is stored in a vertex array (Figure 3(f)), which can be used directly for rendering. Since this information is not needed for computation we only make it available to the rendering part of our pipeline. Besides the $(Lat, Lon)$-coordinate, the vertex also encodes the index into the ensemble data. Second, the actual sea surface height information of the ensemble is stored as a stack of linear arrays, each keeping a single ensemble member. For easier handling a three dimensional array is allocated on the GPU. (Figure 3(b)). Each of the linear arrays corresponding to one ensemble member is then laid out in a two dimensional layer of this three dimensional array. To pack the data tightly the $(x, y)$-coordinate only corresponds to the index and is not correlated with the actual $(Lat, Lon)$-position. A handle to the array is passed to OpenCL for the statistical analysis and another one, pointing to the same location in memory, as a texture to the OpenGL part of the pipeline. By sharing the data between computation and rendering we can avoid costly data transfer from the CPU memory to the GPU memory after the initial upload. Since we can easily index single members in the three dimensional texture we can also compute and visualize statistics for any desired subset of the data without restructuring or transferring additional data. By separating the positional information from the actual simulation data and laying out the simulation data for each member in a two dimensional array as described above we can reuse large parts of the pipeline as described by Höllt et al (2014).

***Statistical Analysis.*** The statistical analysis is carried out separately for each position in the grid. Since no information from neighboring grid cells is needed the statistics can be computed for all positions in parallel, making it a great match for modern GPUs with hundreds to thousands of cores. For each position we compute a histogram and derive a probability density function using the kernel density estimate. We compute several derived height values for each position, such as the mean or median, which, by combining the values of all positions, can be visualized as another surface. In addition we compute the standard deviation and variance, which give a good indication of the uncertainty at each position.

***Rendering.*** Since the statistical analysis is carried out on the GPU all ensemble data are already available in GPU memory. The rendering part of the

pipeline takes advantage of this to enable efficient surface rendering. For example, for creating the surface geometry we do not create geometry for every possible surface, but rather we use a single vertex buffer containing only the indexed positional information as described above, and then inject the SSH information from the data already available on the GPU. The rendering itself is then divided into three stages. First, using a vertex shader, the $z$-value of each vertex is set using the ensemble data directly, or the derived statistics. The value can be looked up using the index of the vertex. The vertex shader is also used to assign color to each vertex using a user-defined lookup table. The second stage is purely for meta information. A geometry shader is used to compute the nearest vertex for each position inside each cell. This information is used for example to quickly find the closest position with available data when the user selects a position on screen. The third and final stage uses a fragment shader to apply additional texturing to the final surface, for example shading, to improve depth perception in the 3D rendering.

The rendering pipeline is used in the 3D view, as well as in the 2D view, to provide real time updates. It is additionally used to render meta information like the closest vertex map described above offscreen.

***Statistical Analysis and Rendering Performance.*** The performance of our analysis and computation pipeline is mostly limited by the computation of the statistics as modern GPUs can throughput several billion triangles per second allowing rendering triangle meshes with millions of triangles with real time refresh rates. An in-depth analysis of the computation times (albeit for different data) including a comparison between computation on the CPU and GPU can be found in our previous work. Table 1 in Höllt et al (2014) shows that all statistics can be updated at least sixty times per second, for a dataset consisting of roughly 57.000 nodes and 50 surfaces (members) per time step (nearly ten times the amount of data compared to the dataset used in the case study in Section 4) using off-the-shelf mid-range graphics hardware. This allows instant feedback for all user interactions at any time.

The performance of the statistics calculation is virtually identical for structured and unstructured data, like the dataset presented in our case study in Section 4. When the statistic can be derived from the histogram, performance scales linearly with the numbers of nodes. When the raw data is needed it is also dependent on the number of ensemble members. Since usually only a single assimilation cycle is analyzed in full at a time the number of cycles has effectively no impact on the performance.

However, in the current form, we assume the complete data of the selected parameter set (spatial dimensions, time and members) to be present in GPU memory, making memory a limiting factor. Today's high-end graphics card have up to 16GB of available memory, posing a hard limit for this approach. To handle data bigger than available memory a viable option would for example be a streaming approach. If the number of members is larger than the number of bins used for the histogram the histogram can be computed by streaming the data through the GPU. Then, if it fits into available memory, only the

histogram can be stored on the GPU and other statistics can be derived from the histogram (with a small loss in precision).

***Interaction.*** The described visualization techniques give a very good impression of the quantitative variation in the data. Detailed information on the surface distribution can be gained by animating through or manually selecting individual surfaces from the ensemble. However, it is hard to obtain a good impression of the complete distribution this way. We therefore show the histogram and pdf for a selected position in a separate view (Figure 1(c)). The position to investigate can be picked directly in the 3D and 2D views.

The combination of the analysis and visualization pipeline on the GPU allows efficient implementation of several features to enhance the exploration of the data. An example for this can be seen by a more detailed look at what we call visualization driven statistical analysis as discussed in Section 3.1. Assuming the user wants to switch from visualizing the mean surface to the median surface, all that is needed is to send a signal to the GPU to compute the median surface. Based on the currently selected ensemble range the median is computed for each point of the grid, resulting in an update of the corresponding surface texture. The next time the view is refreshed the updated texture is automatically used for the vertex displacement in the vertex shader, resulting in the desired visualization. Note that no data transfer between CPU and GPU is needed, besides a single value, setting the active statistic to the median, no geometry needs to be generated and very few CPU cycles are used, leaving the CPU free for other tasks.

Another, even simpler example, is the visualization of a single ensemble member. All that needs to be done here is setting the pointer for the displacement texture directly to the position of this surface in the heightfield texture and everything else works automatically the next time the screen is refresehd. This makes it essentially free to animate over ensemble members by simply moving the pointer in GPU memory. Brown (2004) presents how animation can be used for uncertainty visualization. Simply put, in our case animating over all SSH values will show a steady surface in certain areas, while uncertain areas will vary strongly over time.

While animation and other techniques, like color mapping, can give a good impression of the quantitate variation in the ensemble, it can be hard to get detailed information about the distribution. Therefore we allow the user to select any position and show the corresponding histogram in a separate view (Figure 1(c)). The desired position can be selected by simply picking in any of the spatial views, but the system can also update the histogram continuously while the user moves the mouse over the spatial domain. Therefore we get the index of the datapoint closest to the picked position by a simple lookup in the closest vertex map described above. This makes the interaction very easy and quick as no search in the data needs to be performed, enabling the continuous updates.

***Integration.*** Compared to typical workflows one major advantage of the proposed system is the tight integration of computation and the different visualizations paired with interactive updates in all views. Using our system the user can compare different simulation runs using animation, suspicious simulation runs can be easily detected by visual inspection so the user can exclude them from the dataset. In parallel the system provides live updates of the statistics and visualization without any manual reprocessing of the data. Interactive zooming and panning makes it easy to change the focus area and visualize the data at the needed detail level. Probing using our linked views allows on demand detail inspection in real-time.

## 4 Case Study

In this section we present our system as applied to a real world scenario using a simulation of Hurricane Ike (Berg, 2009). Ike's path took it from the Atlantic, through the Caribbean, traversing the Gulf of Mexico where it reached its peak intensity as a category 4 storm, and finally made landfall on September 13, 2008 as a category 2 storm on the upper Texas coastline (compare Figure 5).

In order to perform the assimilation experiments ADCIRC was run in a hindcast and a forecast configuration. The hindcast configuration utilizes a high resolution grid made up of $3,322,439$ nodes and $6,615,381$ elements

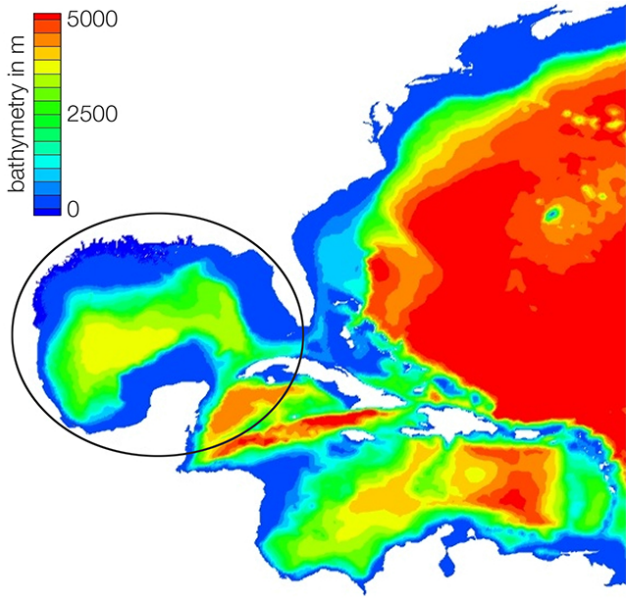


**Fig. 4** Western North Atlantic domain and bathymetry. The Gulf of Mexico is circled in black (modified from Butler et al (2012)).

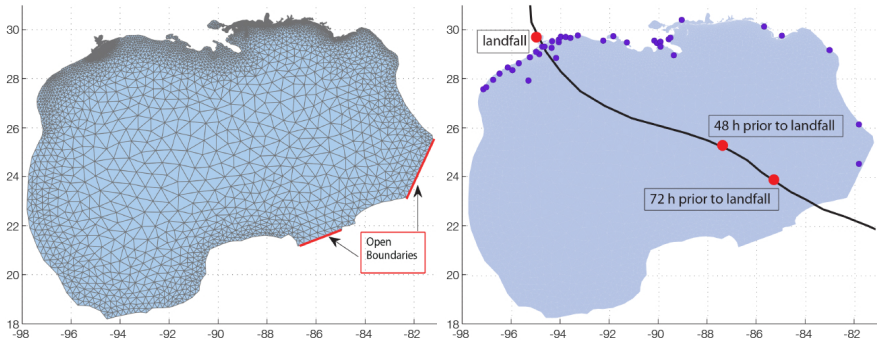


**Fig. 5** Discretization of the Gulf of Mexico domain (left) adapted from Butler et al (2012). The grid contains 8006 nodes and 14, 269 elements. The figure on the right shows the track of Hurricane Ike (black curve) with 53 observation stations indicated by the purple dots.

and data assimilated storm wind fields provided by Ocean Weather, Inc. The time step in the hindcast configuration was 1 second. This configuration's domain covers all of the Gulf of Mexico along with portions of the western Atlantic, see Figure 4. The forecast configuration is comprised of a coarser resolution grid consisting of only 8006 nodes and 14, 269 elements that only covers the Gulf of Mexico and uses a time step of 10 seconds. The forecast configuration uses the SEIK filter to generate the forecast ensemble. Instead of the detailed storm fields a parameterized storm was used based on the model from (Holland, 1980) and best-track data from the NOAA storm archive `ftp://ftp.nhc.noaa.gov/atcf/archive/`.

The hindcast configuration is considered for these experiments as a true representation of the event. Discrepancies between the hindcast configuration and the perturbed versions of the prediction are attributed to model error. Observations extracted every 2 hours from 43 stations (as shown in Figure 5) from the hindcast simulation are then assimilated into the coarser forecast model using the SEIK filter. After a 24 hour ramp-up interval between September 9th, 2008 at 0:00 UTC and September 10th, 2008 at 0:00 UTC data is assimilated every two hours from the hindcast configuration until September 14th, 2008 at 6:00 UTC (one day after landfall) resulting in 51 assimilation steps. The filter itself is initialized by evaluating an ensemble of 40 state vectors from the hindcast configuration (obtained by empirical orthogonal function analysis presented in Hoteit et al (2013)) and projected appropriately onto the coarser grid. The ensemble size was chosen as a reasonable compromise between computational cost and a representative initial ensemble for this study.

### 4.1 Visualization and Analysis of the Results

A typical analysis of the forecast using our visualization system starts with a spatial inspection via the 2D or 3D views. Figure 6 shows a zoom in on

Galveston Bay near Houston, TX in the 3D view. While most of the area demonstrates low variation within the ensemble (indicated by the yellow to light green color), the region near the East Bay exhibits a large standard deviation (blue tone). For further inspection, the user can point into this area and the histogram at the selected position is presented. The distribution histogram for this position (Figure 6 bottom) shows a large spread between +1 m and −1.6 m.

Figure 7 demonstrates additional examples of this type of visual inspection of distributions at different spatial and temporal samples. We picked three exemplary positions in Galveston Bay that show a larger variance than the surrounding area. The distributions at these three positions (as well as the example shown in Figure 6) exhibit notably different characteristics.

Lets consider Figure 6 and Figure 7(a) first. The variance at both positions is large, with nearly the same absolute values (the color coding for all positions maps to the same variance values). The distribution in Figure 6 is widely spread with rather large gaps in between the different simulation runs. This is an indicator that large uncertainty may be present at this point in space and time. The geospatial visualization in Figure 7(a) exhibits similar characteristics as the one in Figure 6. By just looking at the color-coded standard

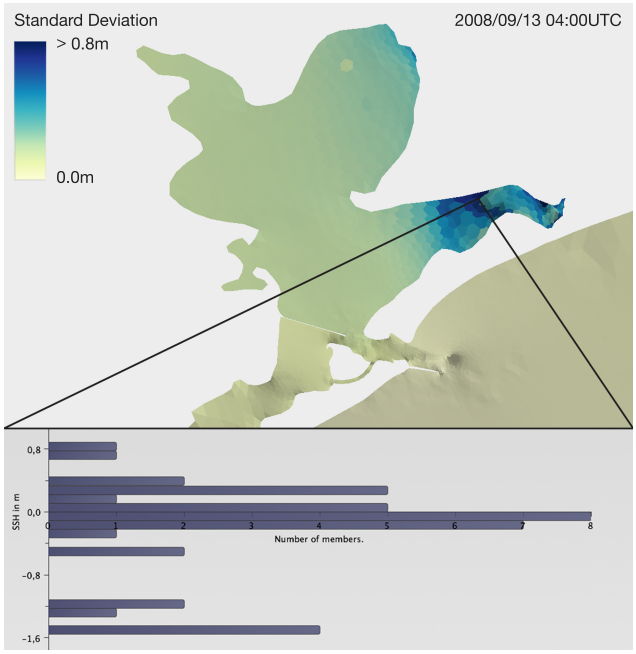


**Fig. 6 Spatial and Distribution Inspection.** The Figure shows a combination of the the 3D spatial view used for the spatial inspection and the histogram view used for detail inspection of the distribution. Note that lighting to enhance 3D structures slightly darkens the colormap.

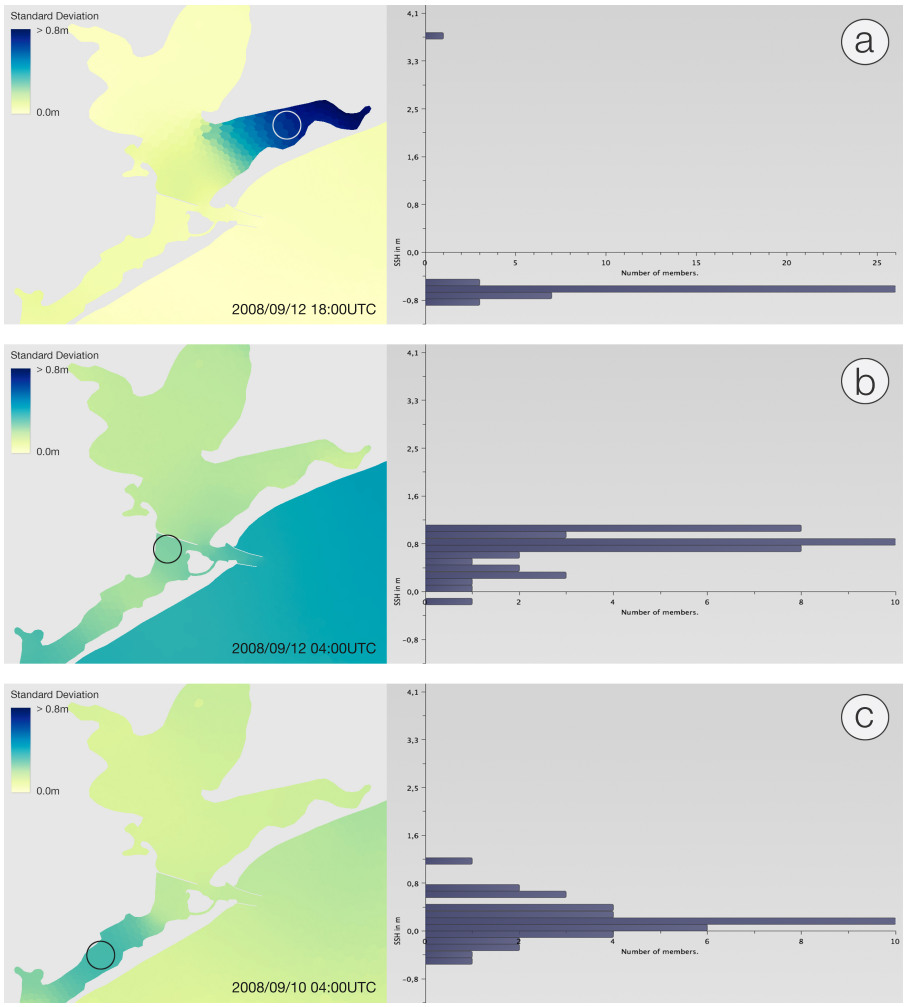


**Fig. 7 Spatial and Distribution Examples** Further examples, showing the use of the histogram in combination with the spatial view. Clearly visible is the large variance in (a) caused by a single outlier. Note that we did not use lighting in these examples to make sure the standard deviation values are not obfuscated.

deviation one might expect similar distributions in the ensembles. However, the histogram in Figure 7(a) exhibits a different distribution, even though the absolute standard deviation value is similar. 39 of 40 simulation runs fall between $-50$ cm and $-90$ cm sea surface height and the large value for the variance is caused by a single outlier at 370 cm. Such a distribution is more likely an indicator of an outlier ensemble member rather than large uncertainty. This could easily be detected using our interactive histogram inspector and might have gone unnoticed when only examining mean and standard deviation.

The positions in Figures 7(b) and (c) exhibit less standard deviation than the first two with only subtle differences in their characteristics. The most significant difference being the fact that the distribution in Figure 7(b) is strongly skewed towards the larger SSH values, while the peak of the histogram in Figure 7(c) is in the center. While this observation is of less importance than the one described above, it would also not be visible by examining mean and variance, only. In our system, the skewness can also be visualized by the surface coloring, giving the user a second way to find these differences.

Moving to a temporal view of the ensemble, the proposed system provides views of the complete time series. The example in Figure 8 shows the complete temporal analysis of two positions in Galveston Bay, chosen in the 2D view on top by simply dropping a pin at each position. The time series view (bottom) shows the pdf of each distribution, for each time step and for both positions. The distributions for both positions are mapped to a glyph according to Figure 2 and the glyphs are assembled on the time axis (x) to give an overview of the complete time-series. Besides the large peak towards the end, corresponding to the landfall of Hurricane Ike, there are several more subtle details which could be of interest. Assimilation cycles seven to eleven (Sept. 10, 2008, 12:00 – 20:00 UTC) exhibit unusually large variations for both positions (indicated by the elongated glyphs). This behavior can be attributed to Hurricane Ike entering the Gulf of Mexico a few hours earlier. The hurricane passed Cuba before the very first assimilation cycle causing a first small rise of the sea surface, which proceeded through the Gulf and reached the Texan coast around assimilation cycle six. This slight rise of the sea level is not only visible in the larger mean values at the selected positions for the following cycles, but is also the cause for the large uncertainty, visible in the time-series view.

The following time steps exhibit very little variance (compact glyphs). Also, remarkable is the small but steep jump in the SSH between assimilation cycles 22 and 23 (Sept. 11, 2008, 18:00 – 20:00 UTC). This might be caused by the forerunner surge, although we did not expect to capture it with the coarse model described above. Also visible is the progress of the surge. Besides being close spatially, Position C1 is constantly one cycle behind C2, most notably in the peak, which occurs at time step 41 (Sept. 13, 2008 at 08:00 UTC) at C2 and time step 42 (Sept. 13, 2008 at 10:00 UTC) at C1.

Figure 9 shows another example for the time series view. We compare two positions, one in the East Bay and one in the ship channel. The first 25 assimilation cycles show similar behavior for both positions with little change in the sea surface height. Similar to the positions described in Figure 8 these positions and cycles exhibit very little variance except for cycles seven to eleven (Sept. 10, 2008, 12:00 – 20:00 UTC). Interesting is the split after cycle 25 (Sept. 12, 2008, 00:00 UTC). In the ship channel (right side of the glyphs) the sea surface rises steadily until it hits its peak around cycle 41 (Sept. 13, 2008, 08:00 UTC). In contrast, the sea surface in the East Bay drops slowly until assimilation cycle 35 (Sept. 12, 2008, 20:00 UTC). The following five cycles exhibit a wide spread in the simulation results (see the elongated glyphs),

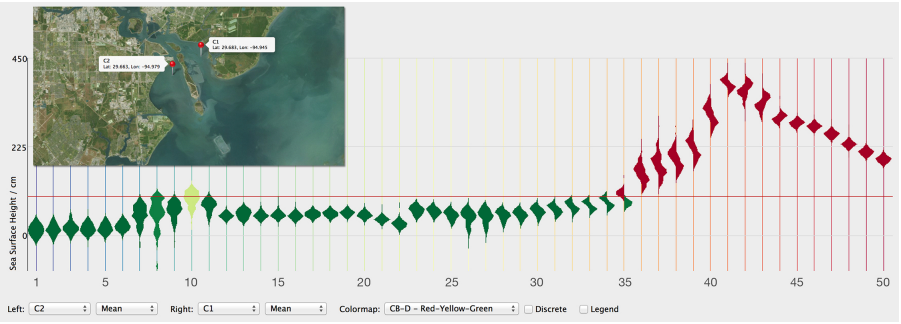


**Fig. 8 Spatial and Time Series Views.** The time series view used for comparing two positions, selected in the 2D view by dropping pins. The arrival of the surge can clearly be seen by the peak in the later time steps. One interesting fact is that position C1 (right side of the glyph) peaks roughly one assimilation cycle (3h) after C2 (left side).

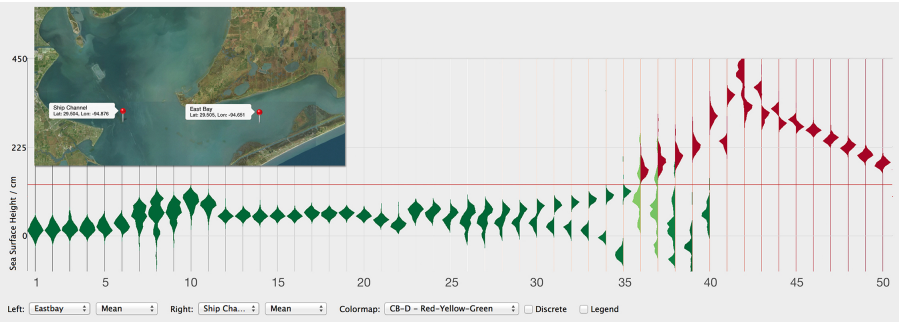


**Fig. 9** Comparing **East Bay and ship channel** in the Time Series View. The figure shows a comparisons of an exemplary position in the East Bay with one in the ship channel (pins in the top view). The left side of the glyphs is mapped to the East Bay, while the right side shows the ship channel. In the first 25 assimilation cycles and after cycle 45 the glyphs are roughly symmetric, indicating similar behavior. After cycle 25 the sea surface height rises steadily in the ship channel, while it falls in the East Bay, before a steep jump after cylce 40. Most interestingly assimilation cycles 36 to 40 exhibit a large amount of variation in the East Bay, indicated by the elongated glyphs.

indicating a large amount of uncertainty. The split of these two positions in the visualization clearly shows the east to west surge within the bay before landfall. However, the large uncertainty, especially in the East Bay also indicates that this surge was not efficiently predicted with all parameter settings. After cycle 40 (Sept. 13, 2008, 06:00 UTC) there is a large jump in the sea surface height, reaching its maximum at cycle 42 (Sept. 13, 2008, 10:00 UTC), with simulation runs with results above 4.5 meters. After this, both positions exhibit similar behavior.

## 5 Conclusions

We introduced a novel, integrated system for interactive visual analysis of storm surge predictions. Based on the work of Höllt et al (2013b, 2014) we present a system adapted to the specific requirements for storm surge visualization. Using multiple linked views and visualization techniques tailored to the problem at hand, our system allows detailed inspection and analysis of storm surge ensembles and their uncertainties.

We demonstrate the application of our system using a case study of Hurricane Ike. The case study clearly shows the usefulness of our system in a real world scenario. Using the completely GPU-based computation and visualization pipeline our system allows interactive visual inspection of complex big data. The interactive probing and our ensemble distribution histogram view allow the user to efficiently obtain detailed information of the distribution of the ensemble. As shown in the example in Section 4.1 this allows quick identification of suspicious simulations without plotting the outputs one by one to find outliers. The use-case scenario also shows that our system allows the identification of important features such as the east west surge in Galveston Bay before Hurricane Ike's landfall, and their corresponding uncertainties.

For the future we will integrate wetting and drying into the simulations and visualization framework to aid in the decision making process. We will also apply the system to other extreme events applications, such as tsunamis and debris flow.

**Acknowledgements** We would like to thank the anonymous reviewers for the constructive comments. Research reported in this publication was supported by the King Abdullah University of Science and Technology (KAUST).

## References

Altaf MU, Butler T, Luo X, Dawson C, Mayo T, Hoteit I (2013) Improving short range ensemble Kalman storm surge forecasting using robust adaptive inflation. Mon Wea Rev 141:2705–2720

Altaf MU, Butler T, Mayo T, Luo X, Dawson C, Heemink AW, Hoteit I (2014) A comparison of ensemble Kalman filters for storm surge assimilation. Mon Wea Rev p in press

Anderson JL (2001) An ensemble adjustment Kalman filter for data assimilation. Mon Wea Rev 129:2884–2903

Berg R (2009) Tropical cyclone report: Hurricane Ike. National Hurricane Center

Bishop CH, Etherton BJ, Majumdar SJ (2001) Adaptive sampling with ensemble transform Kalman filter. Part I: theoretical aspects. Mon Wea Rev 129:420–436

Blake ES, Landsea CW, Gibney EJ (2011) The deadliest, costliest, and most intense united states tropical cyclones from 1851 to 2010 (and

other frequently requested hurricane facts). NOAA Technical Memorandum NWSNHC-6

Brown JD, Spencer T, Moeller I (2007) Modelling storm surge flooding of an urban area with particular reference to modelling uncertainties: a case study of canvey island, united kingdom. Water Resources Research 43

Brown RA (2004) Animated visual vibrations as an uncertainty visualisation technique. In: Proceedings of International Conference on Computer Graphics and Interactive Techniques in Australasia and South East Asia, pp 84–89

Bunya S, Dietrich J, Westerink J, Ebersole B, Smith J, Atkinson J, Jensen R, Resio D, Luettich R, Dawson C, Cardone V, Cox A, Powell M, Westerink H, Roberts H (2010) A high resolution coupled riverine flow, tide, wind, wind wave and storm surge model for southern louisiana and mississippi: Part i - model development and validation. Mon Wea Rev 138:345–377

Burgers G, van Leeuwen PJ, Evensen G (1998) On the analysis scheme in the ensemble Kalman filter. Mon Wea Rev 126:1719–1724

Butler T, Altaf MU, Dawson C, Hoteit I, Luo X, Mayo T (2012) Data assimilation within the advanced circulation (ADCIRC) modeling framework for hurricane storm surge forecasting. Mon Wea Rev 140:2215–2231

Cubasch U, Santer B, Hellbach A, Hegerl G, Hck H, Maier-Reimer E, Mikolajewicz U, Stssel A, Voss R (1994) Monte carlo climate change forecasts with a global coupled ocean-atmosphere model. Climate Dynamics 10(1-2):1–19

Dietrich J, Westerink J, Kennedy A, Smith J, Jensen RE, Zijlema M, Holthuijsen L, Dawson C, Luettich R, Powell M, Cardone V, Cox A, Stone G, Pourtaheri H, Hope M, Tanaka S, Westerink L, Westerink HJ, Cobell Z (2011a) Hurricane gustav (2008) waves and storm surge: Hindcast, synoptic analysis and validation in Southern Louisiana. Monthly Weather Review 139:2488–2522

Dietrich J, Zijlema M, Westerink J, Holtjuijsen L, Dawson C, Jr RL, Jensen R, Smith J, Stelling G, Stone G (2011b) Modeling hurricane wave and storm surge using integrally-coupled, scalable computations. Coastal Engineering 58:45–65

Dietrich J, Dawson C, Proft J, Howard M, Wells G, Fleming J, Jr RL, Westerink J, Cobell Z, Vitse M, Lander H, Blanton B, Szpilka C, Atkinson J (2013) Real-Time Forecasting and Visualization of Hurricane Waves and Storm Surge using SWAN+ADCIRC and FigureGen, vol 156

Dietrich JC, Bunya S, Westerink JJ, Ebersole BA, Smith JM, Atkinson JH, Jensen R, Resio DT, Luettich RA, Dawson C, Cardone VJ, Cox AT, Powell MD, Westerink HJ, Roberts HJ (2010) A high resolution coupled riverine flow, tide, wind, wind wave and storm surge model for southern louisiana and mississippi: Part ii - synoptic description and analyses of hurricanes katrina and rita. Mon Wea Rev 138:378–404

Djurcilov S, Kim K, Lermusiaux PFJ, Pang A (2001) Volume rendering data with uncertainty information. In: Data Visualization 2001: Proceedings of the Joint Eurographics - IEEE TCVG Symposium on Visualization, pp 243–252

Djurcilov S, Kim K, Lermusiaux PFJ, Pang A (2002) Visualizing scalar volumetric data with uncertainty. Computers and Graphics 26:239–248

El Serafy GY, Mynett AE (2008) Improving the operational forecasting system of the stratified flow in osaka bay using an ensemble kalman filter–based steady state kalman filter. Water Resources Research 44(6)

Evensen G (1994) Sequential data assimilation with a nonlinear quasi-geostrophic model using Monte Carlo methods to forecast error statistics. J Geophys Res 99:10,143–10,162

Ghil M (1989) Meteorological data assimilation for oceanographers. part i: Description and theoretical framework. Dynamics of Atmospheres and Oceans 13(3):171–218

Griethe H, Schumann H (2006) The visualization of uncertain data: Methods and problems. In: Proceedings of SimVis

Heap NS (1983) Storm surges 1967–1982. Geophys J R Astron Soc 74:331–376

Heemink A, Kloosterhuis H (1990) Data assimilation for non-linear tidal models. International journal for numerical methods in fluids 11(8):1097–1112

Heemink AW (1986) Storm surge prediction using kalman filtering

Helton J (2008) Uncertainty and sensitivity analysis for models of complex systems. In: Computational Methods in Transport: Verification and Validation, Lecture Notes in Computational Science and Engineering, vol 62, pp 207–228

Hintze JL, Nelson RD (1998) Violin plots: A box plot-density trace synergism. The American Statistician 52(2):181–184

Holland G (1980) An analytic model of the wind and pressure profiles in hurricanes. Mon Wea Rev 108:1212–1218

Höllt T, Chen G, Hansen CD, Hadwiger M (2013a) Extraction and visual analysis of seismic horizon ensembles. Eurographics 2013 Short Papers pp 69–72

Höllt T, Magdy A, Chen G, Gopalakrishnan G, Hoteit I, Hansen CD, Hadwiger M (2013b) Visual analysis of uncertainties in ocean forecasts for planning and operation of off-shore structures. In: Proceedings of the IEEE Pacific Visualization Symposium, pp 59–66

Höllt T, Magdy A, Zhan P, Chen G, Gopalakrishnan G, Hoteit I, Hansen CD, Hadwiger M (2014) Ovis: A framework for visual analysis of ocean forecast ensembles. IEEE Transactions on Visualization and Computer Graphics 20(8):1114–1126

Hope ME, Westerink JJ, Kennedy AB, Kerr PC, Dietrich JC, Dawson C, Bender C, Smith JM, Jensen RE, Zijlema M, Holthuijsen LH, Luettich RA, Cardone MDPVJ, Cox AT, Pourtaheri H, Roberts HJ, Atkinson JH, Tanaka S, Westerink HJ, Westerink LG (2013) Hindcast and validation of hurricane ike (2008) waves, forerunner, and storm surge. Journal of Goephys Res (Oceans) pp 4424–4460

Hoteit I, Pham DT, Blum J (2002) A simplified reduced order Kalman filtering and application to altimetric data assimilation in Tropical Pacific. Journal of Marine Systems 36:101–127

Hoteit I, Korres G, Triantafyllou G (2005) Comparison of extended and ensemble based kalman filters with low and high-resolution primitive equations ocean models. Nonlinear Processes in Geophysics 12:755–765

Hoteit I, Pham D, Triantafyllou G, Korres G (2008) A new approximate solution of the optimal nonlinear filter for data assimilation in meteorology and oceanography. Monthly Weather Review 136:317–334

Hoteit I, Hoar T, Gopalakrishnan G, Anderson J, Collins N, Cornuelle B, Kohl A, Heimbach P (2013) A MITgcm/DART ensemble analysis and prediction system with application to the gulf of mexico. Dynamics of Atmospheres and Oceans 63:1–23

Houtekamer PL, Mitchell HL (1998) Data assimilation using an ensemble Kalman filter technique. Mon Wea Rev 126:796–811

Johnson CR, Sanderson AR (2003) A next step: Visualizing errors and uncertainty. IEEE Computer Graphics and Applications 23(5):6–10

Kao D, Dungan J, Pang A (2001) Visualizing 2d probability distributions from eos satellite image-derived data sets: a case study. In: Proceedings of the IEEE Visualization Conference, pp 457–560

Kao D, Kramer M, Love A, Dungan J, Pang A (2005) Visualizing distributions from multi-return lidar data to understand forest structure 42(1):35–47

Kennedy A, Gravois U, Zachry B, Westerink J, Hope M, Dietrich J, Powell M, Cox A, Luettich R, Dean R (2011) Origin of the hurricane ike forerunner surge

Lermusiaux PFJ, Chiu CS, Gawarkiewicz GG, Abbot P, Robinson AR, Miller RN, Haley PJ, Leslie WG, Majumdar SJ, Pang A, Lekien F (2006) Quantifying uncertainties in ocean predictions. Oceanography 19:90–103

Love A, Pang A, Kao D (2005) Visualizing spatial multivalue data. IEEE Computer Graphics and Applications 25(3):69–79

Luettich R, Westerink J (2005) ADCIRC: A parallel advanced circulation model for oceanic, coastal and estuarine waters. Users manual for version 45.08 available at `www.adcirc.org/document/ADCIRCtitlepage.html`

Luo A, Kao D, Pang A (2003) Visualizing spatial distribution data sets. In: Proceedings of the Symposium on Data Visualisation, pp 29–38

Malanotte-Rizzoli P, Young RE, Haidvogel DB (1989) Initialization and data assimilation experiments with a primitive equation model. Dynamics of atmospheres and oceans 13(3):349–378

Munshi A, Gaster B, Mattson TG, Fung J, Ginsburg D (2011) OpenCL Programming Guide. Addison-Wesley Professional

Murty TS, Flather RA, Henry R (1986) The storm surge problem in the bay of bengal. Progress in Oceanography 16(4):195–233

Nerger L, Janjić T, Schröter J, Hiller W (2012) A unification of ensemble square root Kalman filters. Mon Wea Rev 140:2335–2345

Pang AT, Wittenbrink CM, Lodha SK (1997) Approaches to uncertainty visualization. The Visual Computer 13:370–390

Pfaffelmoser T, Reitinger M, Westermann R (2011) Visualizing the positional and geometrical variability of isosurfaces in uncertain scalar fields. Computer Graphics Forum 30(3):951–960

Pham DT (2001) Stochastic methods for sequential data assimilation in strongly nonlinear systems. Mon Wea Rev 129:1194–1207

Pöthkow K, Hege HC (2011) Positional uncertainty of isocontours: Condition analysis and probabilistic measures. IEEE Transactions on Visualization and Computer Graphics 17(10):1393–1406

Pöthkow K, Weber B, Hege HC (2011) Probabilistic marching cubes. Computer Graphics Forum 30(3):931–940

Potter K, Wilson A, Bremer PT, Williams D, Doutriaux C, Pascucci V, Johnson CR (2009) Ensemble-Vis: A framework for the statistical visualization of ensemble data. In: IEEE Workshop on Knowledge Discovery from Climate Data: Prediction, Extremes and Impacts, pp 233–240

Rhodes PJ, Laramee RS, Bergeron RD, Sparr TM (2003) Uncertainty visualization methods in isosurface rendering. In: EUROGRAPHICS 2003 Short Papers, pp 83–88

Riveiro M (2007) Evaluation of uncertainty visualization techniques for information fusion. In: Proceedings of the 10th International Conference on Information Fusion, pp 1–8

Rost RJ, Licea-Kane BM, Ginsburg D, Kessenich JM, Lichtenbelt B, Malan H, Weiblen M (2009) OpenGL Shading Language. Addison-Wesley Professional

Sanyal J, Zhang S, Dyer J, Mercer A, Amburn P, Moorhead RJ (2010) Noodles: A tool for visualization of numerical weather model ensemble uncertainty. IEEE Transactions on Visualization and Computer Graphics 16(6):1421 – 1430

Shreiner D, Sellers G, Kessenich JM, Licea-Kane BM (2013) OpenGL Programming Guide: The Official Guide to Learning OpenGL. Addison-Wesley Professional

Sørensen JVT, Madsen H (2006) Parameter sensitivity of three kalman filter schemes for assimilation of water levels in shelf sea models. Ocean Modelling 11(3):441–463

Tippett MK, Anderson JL, Bishop CH, Hamill TM, Whitaker JS (2003) Ensemble square root filters. Mon Wea Rev 131:1485–1490

Westerink JJ, Luettich RA, Feyen JC, Atkinson JH, Dawson CN, Roberts HJ, Powell MD, Dunion JP, Kubatko EJ, Pourtaheri H (2008) A basin to channel scale unstructured grid hurricane storm surge model applied to southern louisiana. Mon Wea Rev 136:833–864

Whitaker JS, Hamill TM (2002) Ensemble data assimilation without perturbed observations. Mon Wea Rev 130:1913–1924